analytical chemistry

pubs.acs.org/ac Article

Light-Addressable Electrochemical Sensing with Electrodeposited n-Silicon/Gold Nanoparticle Schottky Junctions

Irina M. Terrero Rodríguez, Alexandra J. Borrill, Katherine J. Schaffer, Jocelyn B. Hernandez, and Glen D. O'Neil*

Cite This: *Anal. Chem.* 2020, 92, 11444−11452 Read Online

ACCESS | Metrics & More | Article Recommendations | Supporting Information

ABSTRACT: Light-addressable electrochemical sensors (LAESs) are a class of sensors that use light to activate an electrochemical reaction on the surface of a semiconducting photoelectrode. Here, we investigate semiconductor/metal (Schottky) junctions formed between n-type Si and Au nanoparticles as light-addressable electrochemical sensors. To demonstrate this concept, we prepared n-Si/Au nanoparticle Schottky junctions by electrodeposition and characterized them using scanning electron microscopy, cyclic voltammetry, and electrochemical impedance spectroscopy. We found that the sensors behaved almost identically to Au disk electrodes for the oxidation of an outer-sphere redox couple (ferrocene methanol) and two inner-sphere redox couples (potassium ferrocyanide and dopamine). In buffered dopamine solutions, we observed broad linear ranges and submicromolar detection limits. We then used local illumination to generate a virtual array of electrochemical sensors for dopamine as a strategy for circumventing sensor fouling, which is a persistent problem for electrochemical dopamine sensors. By locally illuminating a small portion of the photoelectrode, many measurements of fouling analytes can be made on a single sensor with a single electrical connection by moving the light beam to a fresh area of the sensor. Altogether, these results pave the way for Schottky junction light-addressable electrochemical sensors to be useful for a number of interesting future applications in chemical and biological sensing.

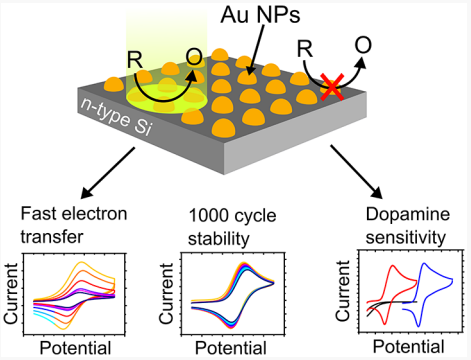

Light-addressable electrochemical sensing (LAES) is a technique which uses light to trigger a spatially and temporally selective electrochemical reaction on the surface of a semiconducting photoelectrode.[1,2] The basic operating principle of LAES using an n-type semiconductor and a high work function metal is shown in Scheme 1a. Here, an n-type Si photoanode is coated with Au nanoparticles (NPs) and placed in a solution of a reduced redox species, R. In the dark regions of the electrode under an appropriate applied potential, the oxidation of R to O is not possible because the semiconductor is in depletion. When a semiconductor is in depletion, the concentration of minority charge carriers (i.e., holes for n-type materials or electrons for p-type materials) is insufficient to enable redox reactions at the sensor/solution interface (Scheme 1b).[3−8] For n-type semiconductors, a LAES will be in depletion at potentials more positive that the flat-band potential, E_{FB}. For p-type semiconductors, depletion conditions are met when the electrode is biased at potentials more negative than E_{FB}. In the areas that are illuminated with light that has higher energy than the semiconductor band gap, R can be oxidized to form the product O because electron−hole pairs generated in the semiconducting layer are separated and transported to the interfaces—holes are transported to the sensing interface while the electrons are transferred to the Ohmic connection.[9] LAES has led to new applications in electrochemical sensing,[10] imaging,[11−13] surface pattern-

Scheme 1. (a) Schematic Representation of n-Si/AuNP NP LAES Showing Oxidation in the Illuminated Portions and (b) n-Si/AuNP Band Diagram Schematic

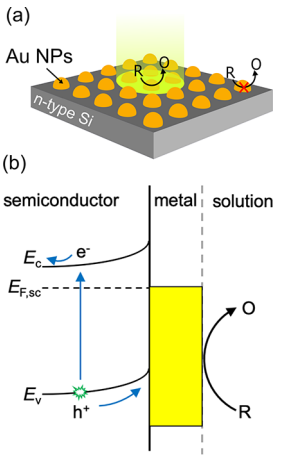

Received: June 12, 2020
Accepted: July 17, 2020
Published: July 17, 2020

https://dx.doi.org/10.1021/acs.analchem.0c02512
Anal. Chem. 2020, 92, 11444−11452

ing,[14,15] and even fundamental studies of semiconductor photoelectrochemistry.[16]

Designing LAES for practical applications is considerably more challenging than designing electrochemical sensors based on metallic or carbon electrodes because the semiconductor/electrolyte interface is more difficult to control than a metallic electrode/electrolyte interface.[17] In straightforward cases, voltammetry at a semiconductor/electrolyte interface is influenced not only by mass transport of redox species and electron transfer across the interface but also by potential corrosion of the semiconductor in an aqueous electrolyte as well as carrier dynamics within the semiconductor.[18] Each of these factors must be carefully controlled in order to have sensors that give reliable data and are reproducible.

The vast majority of recent LAES studies use a Si electrode modified with a monolayer of α,ω-diynes that protect the Si interface and provide a route for functionalizing the electrode with redox couples[10−12,19−23] or NPs.[24,25] The pioneering first report from Gooding's group showed ideal electrochemical behavior for surface-bound ferrocene and anthraquinone redox couples,[10] and the sensing surface has been subsequently used for DNA sensing,[10] live cell K^+ imaging,[11] and selective cell capture and release,[23] in addition to probing the fundamentals of charge transfer at the semiconductor/liquid interface.[16] This Si modification scheme has excellent electrochemical performance, stability, and versatility; however, one challenge is that the samples require complex, multistep syntheses to modify the Si surface. In addition, measurement of freely diffusing redox species requires additional modifications or coreactants in solution.[24,25] Other viable approaches employ transition metal oxides (e.g., hematite)[26,27] or quantum dots[28,29] as the semiconductor layer. Transition metal oxides are attractive because they do not corrode in aqueous solutions at anodic potentials, however they typically have poor photoelectrochemical performance compared to Si. It is therefore desirable to devise strategies for making LAES using Si photoelectrodes without a cumbersome protection scheme. To our knowledge, semiconductor−metal (Schottky) junctions have not been adapted for LAES, even though they are widely studied for photoelectrochemical energy conversion,[30,31] and there is vast literature describing the fundamentals of their charge transport.[32] An attractive feature of using Schottky junctions for LAES is that the electrochemical reaction occurs on the metal rather than the semiconductor, and electrochemical reactions on metal surfaces are largely well-understood. A direct consequence is that the systems can be modeled by connecting a semiconducting diode in series with a metal electrode.[7] Another advantage is that Au can be easily functionalized with biological molecules via thiol-Au chemistry.[33]

One unexplored application of LAES is to use the ability to selectively activate discrete areas of the electrode to build virtual arrays that circumvent electrode fouling. Electrochemically induced biofouling is a serious problem that plagues electrochemical sensors[34,35] and is especially problematic in sensing the catecholamine neurotransmitters—even in a buffer.[36] Dopamine is known to foul electrodes by forming polydopamine, an insulating polymer that adsorbs onto the electrode surface and blocks electron transfer across the electrode/electrolyte interface.[37] Numerous solutions have been developed which have targeted this problem, including developing electrode coatings (or other modifications), electrochemical activation of the surface, modifying the electrolyte to contain surfactants, or by using flow systems to minimize contact time with the electrode (reviewed in ref 38). To date, the majority of catecholamine fouling studies have focused on carbon electrodes because they are the electrode of choice for *in vivo* measurements. As a result, relatively little attention is paid to other materials.

Here, we demonstrate that Schottky junctions formed from n-type Si and Au NPs have excellent electrochemical behavior and can be used as LAES. We found that the sensors behaved almost identically to Au disk electrodes for the oxidation of one outer-sphere redox couple (ferrocene methanol) and two inner-sphere redox couples (potassium ferrocyanide and dopamine). We show that n-Si/AuNPNP samples are stable under illumination in an aqueous electrolyte for 1000 cyclic voltammetry cycles using ferrocene methanol (approximately 3 h of continuous use) even though the electrodes are only partially covered with Au NPs. We also found that the sensors had favorable responses toward dopamine at low concentrations. In order to circumvent sensor fouling by dopamine, we used a virtual array format, where a small portion of the LAES is activated by local illumination with a focused light beam. The virtual array format is advantageous because once dopamine fouls a small portion of the sensor, a new sensor can be activated by moving the focused light beam to a new location. The results demonstrate that Schottky junctions between n-Si and Au nanoparticles are suitable for LAES and pave the way for new chemical and biological sensing schemes based on this this platform.

EXPERIMENTAL SECTION

Materials and Solutions. Potassium chloride (KCl), sodium chloride (NaCl), disodium phosphate (Na_2HPO_4), monosodium phosphate (NaH_2PO_4), and potassium ferrocyanide trihydrate ($K_4[Fe(CN)_6]\cdot H_2O$) were from Fisher Scientific and were certified ACS grade. Ferrocene methanol (FcMeOH; 97%) was from Acros Organics. Hydrogen tetrachloroaurate(III) trihydrate ($HAuCl_4\cdot 3H_2O$; 99.99%) was from Alfa Aesar. Dopamine hydrochloride was from Sigma. All chemicals were used as received. Solutions containing FcMeOH were sonicated for 60 min and passed through a 0.2 μm polycarbonate filter before use. All solutions were prepared using 18.2 MΩ·cm water (Millipore Simplicity).

Electrode Preparation. The LAESs used in this study were prepared using n-type Si (100) and highly doped (metallic) p*-Si (100) from Pure Wafer (San Jose, CA). Both wafer types were single-side polished and 500−550-μm-thick. The n-type wafers were doped with phosphorus (resistivity 1−5 Ω·cm), and the p* wafers were doped with boron (resistivity <0.005 Ω·cm). Semiconducting Si has a band gap $E_g \approx 1.1$ eV (≈1100 nm). Ohmic back contacts were prepared by scratching the unpolished side of the wafer with a diamond scribe to remove the native oxide and subsequently contacting a Cu wire using indium solder. The back contacts were insulated by sealing the entire assembly in 3M Electroplater's tape, which included a d = 4 mm circular opening that allowed exposure of the polished front Si surface to the electrolyte.

Au NPs were electrodeposited onto the polished front surface of Si in order to protect the underlying Si surface, establish a rectifying semiconductor-metal junction, and increase the electronic coupling between the semiconductor and redox species, using a modified procedure previously described by Allongue et al.[39] Briefly, the electrode was etched in 40% NH_4F solution (Honeywell, semiconductor grade) for 10 min at room temperature to remove the native oxide. H-

https://dx.doi.org/10.1021/acs.analchem.0c02512
Anal. Chem. 2020, 92, 11444−11452

termination was confirmed by placing a small droplet of water on the surface to confirm hydrophobicity. The electrode was rinsed with copious amounts of DI water prior to electrodeposition. The electrode was biased at −1.9 V vs Ag/AgCl before being dipped in the deposition solution to prevent the formation of SiO_x during exposure to the electrolyte. The deposition solution consists of 0.1 mM $HAuCl_4$, 1 mM KCl, 0.1 M K_2SO_4, and 1 mM H_2SO_4. The deposition was carried out with room lights on, but without direct illumination of the semiconductor surface. Four different deposition times (5, 10, 15, and 20 min) were tested in order to determine if there was a measurable impact on the observed voltammetry.

Electrochemical Measurements. Bulk electrochemical experiments were carried out using a CH Instruments 660C potentiostat or 760E bipotentiostat. All electrochemical measurements were carried out in a 100 mL flat-walled glass electrochemical cell using a three-electrode configuration. A Ag/AgCl electrode served as the reference and a graphite rod or Pt wire as the counter. Au disk electrodes (2 mm diameter) were obtained from CH Instruments (USA). Electrochemical impedance spectra (EIS) for Mott−Schottky measurements were carried out in the dark at 35, 42.5, 50, and 65 kHz in an electrolyte containing 1 mM FcMeOH/0.1 M KCl over an appropriate potential range, typically −0.8 to 0 V vs Ag/AgCl. A separate impedance measurement was made every 20 mV. The space charge capacitance (C_{sc}) was calculated from the impedance data using eq 1:

$$Z'' = \frac{1}{2\pi\nu C_{sc}} \tag{1}$$

where Z'' is the imaginary component of the impedance and ν is the frequency in Hz. Illumination of the semiconductor was provided using a white light LED (AM Scope) with a measured power density of 85 mW cm^{-2}.

Virtual array experiments were performed using a HEKA ELP 1 scanning electrochemical workstation equipped with a PG 160 USB bipotentiostat. The semiconductor was illuminated with a 530 nm (2.3 eV) fiber-coupled LED (M530F2) coupled to a 365 μm diameter fiber optic cable (MHP365L02, Thorlabs), a F240SMA-532 collimator, and a 10× objective (see Section S6 in the Supporting Information for more details). All optical components were purchased from Thorlabs and were housed inside a custom-built dark Faraday cage to eliminate ambient light and minimize electronic noise. The measured power density was ∼200 mW cm^{-2}.

Physical Characterization. Optical microscopy was performed using an AmScope MR400 metallurgical microscope using a 10× objective to check the macroscale homogeneity of the electrodeposited Au NPs. Field emission scanning electron microscopy (FE-SEM) was performed using a Zeiss GeminiSEM 500 on InLens mode operating at 15 kV. Energy-dispersive X-ray spectroscopy (EDX) was performed using a Hitachi S-3400N SEM in secondary electron mode using a 30 kV accelerator voltage.

RESULTS AND DISCUSSION

Surface Characterization. We prepared n-Si/AuNP Schottky junctions by electrodepositing Au on a freshly etched n-type Si (100) electrode using an electrolyte containing 0.1 mM $HAuCl_4$, 1 mM KCl, 0.1 M K_2SO_4, and 1 mM H_2SO_4, as previously described by Allongue et al.[39] Figure 1 shows an FE-SEM image of Au NPs grown on n-Si for minutes at −1.9 V vs Ag/AgCl. Under the electrodeposition conditions, the n-Si surface is partially covered with Au NPs. Statistical analysis of the NPs performed using ImageJ shows that the NPs are 15 ± 6 nm and cover approximately 31% of the surface, and the density of particles on the surface is approximately 1.6 (±0.2) × 10^{11} cm^{-2} (n = 200). Increasing the deposition time to 20 min increased the nanoparticle diameter, surface coverage, and particle density (section S1 in the Supporting Information), but the electrochemical performance of the 5 and 20 min samples was nearly identical in FcMeOH solutions (*vide infra*). EDX analysis confirms that the NPs formed on the surface are Au (Figure S1). These results are similar to those reported by Switzer et al., who deposited continuous epitaxial Au films on n-Si (111) using a similar procedure.[40] However, the films grown on n-Si (111) had coalesced after a 5 min deposition. The differences may be due to the crystal orientation of the substrates used in each study ((100) vs (111)).

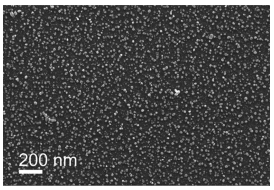

Figure 1. FE-SEM image of n-Si/AuNP LAES prepared by electrodepositing Au NPs for 5 min at −1.9 V vs Ag/AgCl.

n-Si/AuNP Schottky Junction Energetics. We characterized the energetics of the n-Si/AuNP Schottky junction to determine the potential range over which the sensor would be light-addressable by measuring the flat band potential (E_{FB}) and the conduction and valence band edges.[41] E_{FB} is the potential where there is no band bending in the semiconductor and is useful for estimating the approximate voltage range over which the semiconductor layer will be in depletion (and therefore photoactive). Figure 2a shows impedance data (presented as a Mott−Schottky plot) for a 5 min n-Si/AuNP sensor in an electrolyte containing 1 mM FcMeOH and 0.1 M KCl recorded at 35 kHz. Figure S3 in the Supporting Information shows similar plots collected at 42.5, 50, and 65 kHz. The flat band potential of the n-Si/AuNP interface was determined from the x intercept of the Mott−Schottky plot to be −0.66 ± 0.02 V vs Ag/AgCl (n = 4). Using E_{FB}, we estimated the conduction band edge position (E_{cb}) to be −0.93 ± 0.03 V, using eq 2:[42]

$$E_{cb} = E_{FB} + k_B T \ln\left(\frac{N_d}{N_c}\right) \tag{2}$$

where k_B is Boltzmann's constant, N_d is the bulk dopant concentration (= (7.6 ± 0.3) × 10^{14} cm^{-3}, obtained from the slope of the Mott−Schottky plot),[41] and N_c is the effective density of states for the conduction band (= 2.8 × 10^{19} cm^{-3} for Si). We estimated the valence band edge to be 0.17 V vs Ag/AgCl using the conduction band edge and the Si band gap (1.1 eV). Details of the calculations can be found in the Supporting Information, section S2. Taken together, these data suggest that these sensors should be light-addressable when biased at potentials more positive than −0.66 V vs Ag/AgCl.

Electrochemical Characterization of n-Si/AuNP Schottky Junctions. We first characterized the photoelectrochemical behavior of the n-Si/AuNP Schottky junctions using cyclic voltammetry (CV) in FcMeOH, which is an outer-

https://dx.doi.org/10.1021/acs.analchem.0c02512
Anal. Chem. 2020, 92, 11444−11452

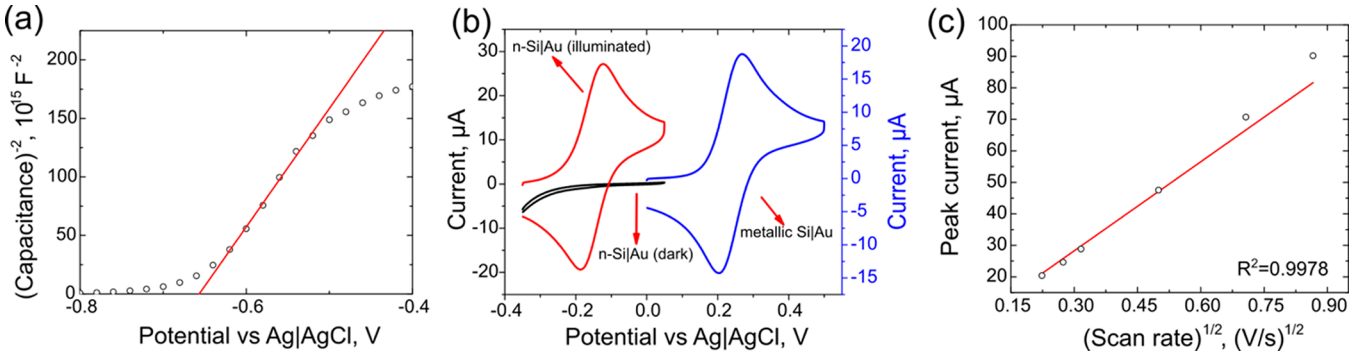

Figure 2. Electrochemical characterization of n-Si/AuNP Schottky junction sensors. (a) Mott−Schottky plot of a n-type Si/AuNP electrode at 35 kHz. (b) CVs of 1 mM FcMeOH using highly doped p*-Si/AuNP electrodes in the dark (blue trace), semiconducting n-Si/AuNP photoelectrodes in the dark (black trace), and fully illuminated semiconducting n-Si/AuNP photoelectrodes (red trace). Scan rate = 0.1 V s^{-1}. (c) Randles−Sevcik analysis of anodic peak current vs the square root of scan rate confirming that diffusion of the reactant is limiting the current response. Dots represent the experimental data, while the solid line represents the theoretical slope calculated using eq 3.

sphere redox couple known to have very fast heterogeneous electron transfer (HET) kinetics.[43] Figure 2b shows CVs of 1 mM FcMeOH using n-Si/AuNP and p*-Si/AuNP control samples in the presence and absence of 85 mW cm^{-2} illumination. First, consider the blue trace in Figure 2b which shows a CV for the oxidation of FcMeOH using a highly doped (metallic) p*-Si/AuNP substrate in the dark. As expected, the electrochemical behavior of this sample is excellent, as demonstrated by the separation of the peak potentials (ΔE_p = 65 ± 2 mV at 0.1 V s^{-1}; n = 4). This demonstrates that the electrodeposition of Au NPs on the surface of Si enables efficient electron transfer across the solid/liquid interface. The black trace in Figure 2b shows the semiconducting n-Si/AuNP photoelectrode in the absence of light. As expected from the Mott−Schottky measurements (Figure 2a), the semiconducting n-Si/AuNP photoelectrode is inactive in the dark (Figure 2b, black trace) because over this potential range the semiconductor is in depletion. Illuminating the entire surface using 85 mW cm^{-2} white light generates electron/hole pairs in the semiconductor which are transported to the Au NPs because of the band bending at the Schottky junction (Scheme 1b). Under illumination, the n-Si/AuNP sample becomes electrochemically active (Figure 2b, red trace). By comparing the black trace to the red trace, the power of this technique is clearly demonstrated because the "turn on" electrochemical signal shows a ≈100× increase upon the addition of light. Compared to the p*-Si/AuNP control, the CV for n-Si/AuNP is shifted toward cathodic potentials by about −0.4 V (note this energy is less than the formal potential of the redox couple). Energy from the absorbed light causes this cathodic photovoltage shift by shifting the electrode potential to more anodic values than those applied by the potentiostat.[2] We varied the electrodeposition time (5, 10, 15, and 20 min) but observed very little effect on the measured photovoltage shift or the CV peak separation, as shown in Figure S4, and for all future studies we employed the 5 min deposition time.

As a control experiment, we also performed CV of FcMeOH using a freshly etched n-Si electrode without Au NPs (Figure S5). Without Au NPs, the electrochemistry is very sluggish. This result suggests that the electron transfer to FcMeOH across the sensor/solution interface likely takes place on the Au particles, rather than the exposed Si.

We also characterized the n-Si/AuNP electrodes using $Fe(CN)_6^{4-}$ to determine if the light-addressable response was limited to FcMeOH and observed very similar results to FcMeOH. These experiments are detailed in section S4 of the Supporting Information.

In order to characterize the mass-transport behavior of the n-Si/AuNP junctions, we performed CV over a range of scan rates (0.05−0.75 V s^{-1}) in FcMeOH. Figure 2c shows a Randles plot of peak current vs the square root of scan rate ($v^{1/2}$). The relationship between peak current and ($v^{1/2}$) is linear (R^2 = 0.9978) and indicates that diffusion of FcMeOH to the n-Si/AuNP Schottky junction is linear, caused by overlapping diffusion fields at each Au NP.[44] This is expected given the high density and close spacing of the Au NPs. The expected gradient of the line was calculated using eq 3:

$$i_p = 268600 n^{3/2} A D^{1/2} c_b v^{1/2} \quad (3)$$

where i_p is the peak current, n is the number of electrons transferred in the reaction (= 1), A is the electrode area (= πr^2; r = 0.20 ± 0.01 cm), D is the diffusion coefficient of the redox species (cm^2 s^{-1}; 7.8 × 10^{-6} cm^2 s^{-1}),[45] c_b is the bulk concentration of the redox species (= 1 × 10^{-6} mol cm^{-3}), and v is the scan rate (V s^{-1}). The gradient from the experimental data (= 100 ± 2 μA s$^{1/2}$ V$^{-1/2}$) agrees reasonably well with the value predicted using eq 3 (= 94 μA s$^{1/2}$ V$^{-1/2}$).

Numerous models have been developed to describe the kinetic behavior of semiconducting photoelectrodes, which are considerably more complex than metallic electrodes.[46] With metallic electrodes, the HET rate is not typically affected by charge transport in the metal. However, with semiconductors, charge transfer, recombination, diode quality, and interfacial properties can all impact the overall rate.[18] On the basis of the shape of the CVs in Figure 2b and the close agreement with the Randles−Sevcik equation (eq 3), we hypothesized that the HET rate constant, k^0, could be measured using the Nicolson method, where the peak-to-peak separation in a CV is related to the dimensionless parameter, ψ.[47,48] This assumption would only account for HET across the metal/solution interface and imply that charge transfer in the semiconductor and across the semiconductor/metal interface is considerably faster than the electron transfer rate. Under most conditions, where the electron transfer kinetics are symmetrical ($\alpha \approx 0.5$) and the diffusion coefficients of the oxidized and reduced species are equal, ψ can be calculated by

https://dx.doi.org/10.1021/acs.analchem.0c02512
Anal. Chem. 2020, 92, 11444−11452

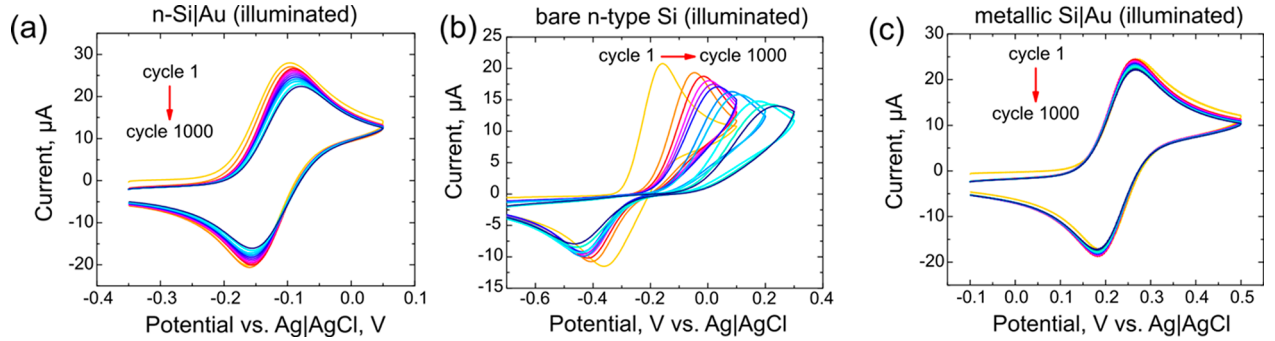

Figure 3. Sensors fabricated using n-Si and Au NPs are stable for at least 1000 cycles. (a) Consecutive CVs of 1 mM FcMeOH and 0.1 M KCl using n-type Si/AuNP electrode under illumination. (b) Consecutive CVs of 1 mM FcMeOH and 0.1 M KCl using a bare n-type Si electrode under full illumination. (c) Consecutive CVs of 1 mM FcMeOH and 0.1 M KCl using a highly doped Si/AuNP photoelectrode under full illumination. Scan rate = 0.1 V s^{-1}, reference electrode = Ag/AgCl, counter electrode = graphite rod.

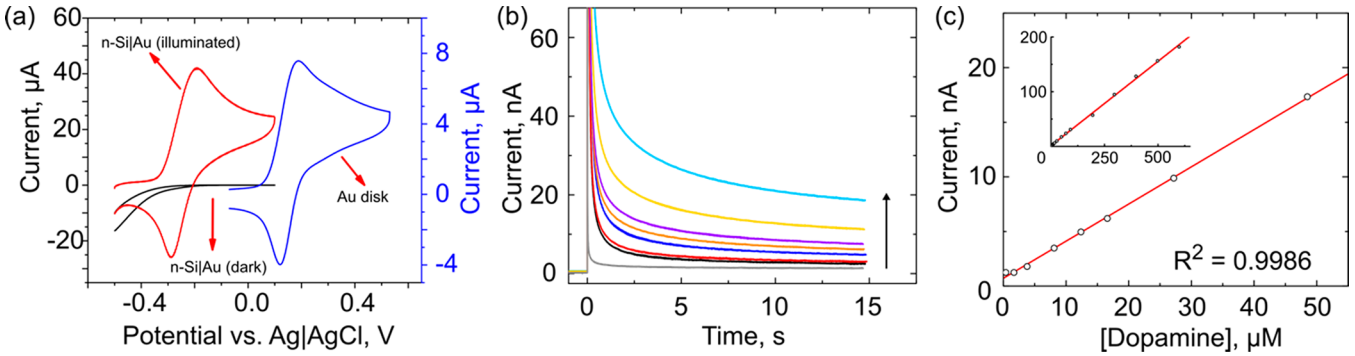

Figure 4. Sensors based on n-Si and electrodeposited Au are light-activated and quantitative for dopamine. (a) CVs of 1 mM dopamine in PBS buffer using Au disk electrode in the dark (blue trace), and semiconducting n-type Si/AuNP photoelectrodes in the dark (black trace) and fully illuminated (red trace). Scan rate = 0.25 V s^{-1}. (b) Light-activated CAs of increasing dopamine concentrations using an n-type Si/AuNP photoelectrode. The arrow indicates increasing concentration and the light gray trace was collected in the absence of dopamine; E = +0.1 V vs Ag/AgCl. (c) Calibration curve for dopamine solutions using the n-Si/AuNP photoelectrode under full illumination. Inset: calibration curve of the full data set (0.4−568 μM).

$$\psi = k^0 \sqrt{\frac{RT}{\pi F D}} \nu^{-0.5} \tag{4}$$

where all of the variables have their usual meanings. The dimensionless parameter is calculated using an empirical relationship that depends on the peak-to-peak separation:[49]

$$\psi = \frac{-0.6288 + 0.0021 n \Delta E_p}{1 - 0.017 n \Delta E_p} \tag{5}$$

The HET rate constant for FcMeOH was determined to be 5.0 (±0.4) × 10^{-2} cm s^{-1} and was calculated from the gradient of a plot of ψ versus $\nu^{-1/2}$ (Figure S7b). As a control experiment, we determined the HET rate constant to be 3.2 (±0.3) × 10^{-2} cm s^{-1} using electrodes fabricated using metallic p*-Si/AuNP (Figure S7e). Note the metallic p*-Si samples do not require generation and separation of carriers. The two k^0 values are similar, supporting our hypothesis that k^0 could be estimated by only considering electron transfer across the metal/solution interface.

Stability of n-Si/AuNP Schottky Junctions. Si photoelectrodes are normally unstable in aqueous electrolytes because the Si corrodes to SiO_x at potentials and solution conditions typically encountered in electroanalysis.[50] We studied the stability of the Au NP-coated Si photoelectrodes by performing CV for 1000 cycles at 0.1 V s^{-1} in aqueous FcMeOH solutions over ≈3 h. Figure 3 shows the first, 100th, 200th, 300th, 400th, 500th, 600th, 700th, 800th, 900th, and 1000th cycles for semiconducting n-Si/AuNP, bare n-Si, and metallic p*-Si/AuNP LAES. Figure 3a shows CVs of 1 mM FcMeOH using an n-Si/AuNP Schottky junction LAES. The samples show a slight gradual positive shift of the $E_{1/2}$ value over the 1000 cycles (from −0.129 V to −0.117 V), a minor decay in the current, and a small shift in peak separation (from 66 mV to 75 mV). A detailed analysis of these data is presented in Figure S8. Switzer et al. observed a qualitatively similar trend when using similarly prepared electrodes and attributed the shift to the formation of SiO_x species at the Si surface.[40] It is especially likely that oxides would form on our samples, given that only ≈31% of the samples are protected by the Au NPs. However, the minor changes in both peak currents and ΔE_p suggest that the oxides are thin enough that electrons are effectively able to tunnel from the Au NPs to the Si.[51] In fact, ultrathin oxides are often used to stabilize photoelectrodes for solar fuels applications[30,31,52] and have been shown to increase the stability of NP-coated Si electrodes.[53] Formation of a thin, stable oxide prior to nanoparticle growth is a route which could be used to further increase the lifetime of the sensors.

We performed two control experiments to better understand the results in Figure 3a. First, we tested to see if the presence of Au NPs impacts the stability. Figure 3b shows CVs of a freshly etched n-Si electrode without Au NPs cycled 1000 times. There are dramatic shifts in the CV shape, peak currents, and ΔE_p values that are consistent with oxide-passivation of the Si

https://dx.doi.org/10.1021/acs.analchem.0c02512
Anal. Chem. 2020, 92, 11444−11452

surface.[40] Without Au NPs on the surface, HET between Si and FcMeOH is sluggish, and as the oxide grows, the HET rate dramatically decreases. This showcases the importance of the Au NPs on the sensor performance, which electronically couple the redox species in solution to the semiconductor and are relatively unaffected by the presence of an oxide. Second, we used highly doped (metallic) p*-Si and electrodeposited Au to see how carrier generation/transport impacts the formation of the oxide (Figure 3c). The p*Si−Au samples showed very little decrease in peak current and almost no shift in $E_{1/2}$ or ΔE_p. This suggests that the subtle (∼12 mV) shift in $E_{1/2}$ using the n-Si/AuNP sensors may be due to the formation of an oxide between the Au NPs and n-Si forming a metal−insulator−semiconductor (MIS) junction leading to a shift in the photovoltage.[54]

Photoelectrochemical Sensing of Dopamine. After demonstrating that n-Si/AuNP Schottky junctions have excellent electrochemical behavior in FcMeOH and $Fe(CN)_6^{4-}$, we challenged them by using the more complex $2e^-/2H^+$ oxidation of dopamine in pH 7.4 phosphate buffered saline (PBS). Dopamine has a redox potential of ∼0.2 V vs Ag/AgCl *in vivo*.[55] Therefore, based on the E_{FB} measurements (see above), dopamine should be able to be studied using these n-Si/AuNP Schottky junctions. The blue trace in Figure 4a shows the voltammetric response of a 2 mm diameter Au disk electrode toward 1 mM dopamine in PBS. The black trace in Figure 4a shows the response of the n-Si/AuNP sensor to dopamine in PBS in the dark, and the red trace shows the sensor after illumination. The electrode was active only when illuminated, and negligible current was passed when no illumination was used (Figure 4a, red and black traces, respectively). The large peak separation (ΔE_p = 96 mV) observed for the semiconducting samples indicates sluggish HET kinetics but is qualitatively similar with what we observed using a traditional Au disk electrode (ΔE_p = 71 mV). We suspect that the observed differences are potentially related to *iR* losses caused by the n-Si/AuNP electrodes being much larger than the Au disk electrodes. Control samples prepared using freshly etched n-Si without Au NPs showed a very broad oxidation peak for dopamine which was completely irreversible (Figure S9), again demonstrating the need for efficient electronic coupling between the semiconductor and redox species provided by the Au NPs.

Selectivity of electrochemical dopamine sensors can be problematic because other catecholamine and endogenous species (e.g., ascorbic acid) have similar redox potentials to dopamine.[55] We investigated the selectivity of the sensor by performing CVs in solutions of epinephrine (50 μM), norepinephrine (50 μM), and ascorbic acid (10 mM) which have similar redox potentials to dopamine (Figure S10a−c, respectively). Each redox species displays a well-defined, irreversible voltammogram that is only present upon illumination. CVs of 33 μM dopamine (a lower concentration than each of the other species) are shown alongside the voltammograms for comparison and demonstrate that the photovoltage for dopamine oxidation is significantly greater (i.e., the dopamine onset potential occurs at more cathodic potentials). This behavior offers a voltage window where dopamine could be selectively oxidized in the presence of these alternative redox species.

We tested the ability of the sensor to perform quantitative analysis over the concentration range from 0.4−598 μM using light-activated chronoamperometry (CA). For these experiments, we decreased the electrode diameter from 4 mm to ∼0.5 mm by decreasing the size of the opening on the electroplating tape (see Experimental Section). We hypothesized that a smaller area would lead to smaller and faster-stabilizing backgrounds, which were problematic when we attempted the experiments with larger sensors. In a light-induced chronoamperometry experiment, the sensor is biased at a potential where a diffusion limited response to dopamine would be observed in the light, but where little current flows in the dark (+0.1 V vs Ag/AgCl in these experiments), and the current is recorded continuously. Figure 4b shows the results of the light-induced CA measurements. At $t < 0$, the $i-t$ trace is featureless, highlighting that the entire macroscopic electrode surface is "off" because the Schottky junction is in depletion. At t = 0 s, the electrode is illuminated, and there is a large increase in current originating from the oxidation of dopamine at the electrode surface. Figure 4c shows a calibration curve over the range from 0.4−48.5 μM with excellent linearity (R^2 = 0.9986) and a gradient of 0.340 ± 0.005 μA μM^{-1} (n = 19 points). The linear range of the sensor is very wide (0.4−568 μM; R^2 = 0.9986), as shown in the inset to Figure 4c. The background signals for light-activated CA show very little variation (s_{blank} = 0.4 nA, n = 10), which results in a limit of detection of ∼3 nM (LOD = $3s_{blank}/m$).[56] However, we note that in practice the lowest concentration standard (0.4 μM) yielded a signal that was only slightly smaller than the next calibration point at 1.7 μM (Figure 4c), suggesting that the estimate of 5 nM is too low. An alternative method for estimating the limit of detection is to use the uncertainty of the y intercept in place of the standard deviation of blank signals.[57] Using this approach, we estimate the limit of detection to be 0.8 μM, which we believe is a more reliable description of the performance of the sensor. We hypothesize that there are two linear ranges for the sensor—one which controls the response at concentrations < ∼1 μM and another which controls the response at higher levels. This "two region" response curve is often observed in dopamine sensors[58] and is caused by a changing of the electrochemical mechanism from adsorption-based to diffusion-based. We are currently performing scanning probe measurements to better understand why the response of the sensors changes at very low concentrations and will report those results in due course.

The n-Si/AuNP Schottky-junction LAES performs well in comparison to other LAESs for dopamine. The most relevant comparison is to the work by Seo et al., who used hematite photoelectrodes to detect dopamine and measured a detection limit similar to those reported here (0.7 μM).[26] Unfortunately, in this report, there is no description of the current−voltage behavior of the sensors in dopamine, so it is impossible to determine what other photoelectrochemical processes (corrosion, recombination, solvent oxidation, etc) could also be occurring during measurement. Here, because the voltammetry closely matches the control samples that employ Au only, we have high confidence that there is little to no impact from background or side reactions. The other apt comparison for these sensors is with carbon electrodes, in particular carbon fiber microelectrodes (CFME), which are the standard electrode material for dopamine sensing.[59] When used in fast scan CV (FSCV), CFMEs typically have detection limits of ∼15 nM and a linear range up to 10 μM.[60] The results shown here have a larger detection limit but a much broader linear range. McCarty and co-workers previously observed a broader linear range for Au UMEs compared to CFMEs using FSCV.[61]

https://dx.doi.org/10.1021/acs.analchem.0c02512
Anal. Chem. 2020, 92, 11444−11452

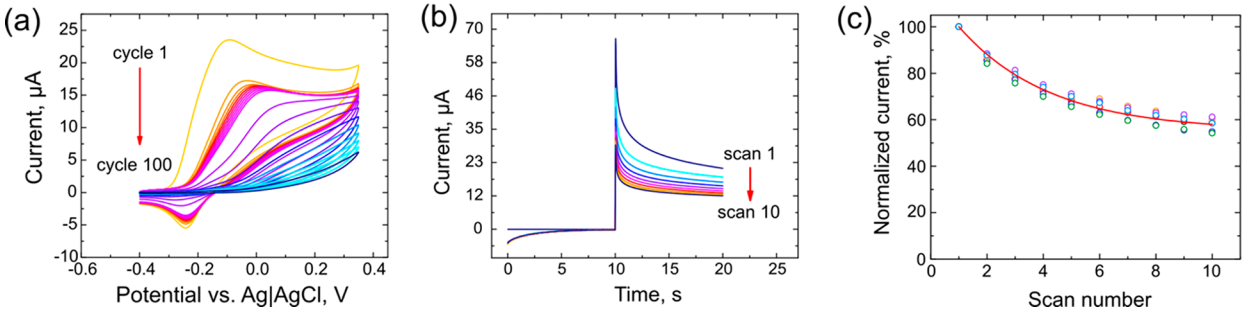

Figure 5. (a) Consecutive CVs of 1 mM dopamine in PBS using n-Si/AuNP Schottky junction under illumination. Scan rate = 0.1 V s^{-1}, reference electrode = Ag/AgCl, counter electrode = graphite rod. (b) Chopped light local illumination *i-t* curve of 1 mM dopamine in PBS at 0.1 V. (c) Relative steady state current % vs scan number for seven different spots. For all measurements, the current was measured at t = 20 s.

Locally Illuminated Electrochemistry to Circumvent Sensor Failure. LAESs have several interesting applications: increasing the density of measurements using a single electrode,[10] imaging of semiconductor surfaces,[11,12] patterning surfaces,[14,15,62] and single cell studies.[11,23] Here, we demonstrate a new application of local illumination whereby we eliminate total sensor failure during electrochemically induced biofouling, which is a common issue with electrochemical sensing of biologically relevant compounds.[34,35] Figure 5a shows the repeated CVs obtained consecutively in 1 mM dopamine in PBS at a scan rate of 0.1 V s^{-1} using an n-Si/AuNP LAES with the entire sensor illuminated. The relatively high concentration of dopamine was chosen to exacerbate dopamine fouling on the sensor. In dopamine, the electrode degraded rapidly, with ∼25% of the current decreasing between the first and second cycles, with complete fouling occurring after 100 cycles. These results are very similar to other electrode materials, such as glassy carbon.[36] The fouled surface completely blocks electron transfer, rendering the sensor useless. Sensor failure was confirmed by performing CVs of FcMeOH, which showed no electron transfer after the 100 dopamine cycles (Figure S11).

We are able to circumvent this problem by creating an array of virtual sensors using localized illumination. Figure 5b shows a light-activated CA curve in 1 mM dopamine at +0.1 V vs Ag/AgCl obtained at a location on a 1 cm^2 sensor that was locally illuminated by a 500 μm diameter beam. Note that only a portion of the sensor surface was illuminated, so the majority of the sensor was "off" during these measurements. The form of the data is similar to that in Figure 4b: in the initial 10 s of each $i-t$ trace there is no light on the sample. After 10 s, a localized light beam (λ = 530 nm; 2.3 eV) was applied to a small region of the sample (∼250 μm radius) using the setup shown in Figure S13. Upon illumination, the diffusion-limited oxidation of dopamine takes place only at the illuminated portions of the sensor, which causes the current to increase. The 20-s cycle was repeated 10 times consecutively at each location. As the cycle number increases, the current transient minimum decreases because polydopamine is forming at *only the illuminated portions* of the sensor (Figure 5b) and blocks the interface for electron transfer. As seen in Figure 5a, when the entire surface was illuminated, the sensor is fouled completely.

Because only a portion of the sensor was illuminated, we simply moved the light beam to a fresh location and repeated the experiment activating a new virtual sensor for each movement of the light beam. Each time the light was moved to a new location, the new location's activity was restored (Figure S12), demonstrating that only the illuminated portion of the sensor was fouling. Figure 5c shows a plot of the relative current (= $i/i_{initial}$ × 100%) vs scan number for seven virtual sensors along with an exponential decay line to guide the eye. The data shows that each new virtual sensor fouls reproducibly. On the basis of the size of the illumination source (0.5 mm diameter), typical minority carrier diffusion lengths in Si (100−300 μm), and the overall size of the sensor (1 cm^2), the upper limit for the number of independent measurements possible is between ∼82 and 204 measurements using a single sensor (assuming the sensor is spatially homogeneous). There is considerable scope for improving this resolution, first by using a smaller light beam and second by employing amorphous Si (or another material with short minority carrier diffusion lengths) as the light absorber.[12]

Increasing the number of measurements per area has several advantages. First, it increases the statistical power available to a single 1 cm^2 sensor. Second, measuring multiple locations on a single sensor could also be used to produce localized activity maps of the sensors which could be correlated with local structural properties and used to identify the most active/high performing motifs for future development. Third, performing calibrations with a virtual array using a fresh location for each calibration point could help eliminate possible fouling induced changes during calibration.

Finally, while the data presented here show that n-Si/AuNP Schottky junctions are excellent choices for LAES, there are several challenges which require future development. The first is that the nature of a rectifying junction necessitates that the sensor will be selective toward oxidations (for n-type) or reductions (for p-type), but not both. However, Gooding's group recently reported intrinsic a-Si LAES which were capable of both oxidation and reduction, but it remains untested with freely diffusing redox couples.[63] Another potential challenge is the need for the Schottky junction to be in depletion, which requires $E^{0\prime}$ to be more positive than E_{FB}. This could potentially limit the number of available redox couples available for analysis.

■ CONCLUSIONS

To date, the vast majority of LAESs employ a chemically modified Si surface that includes a tethered redox molecule. In this contribution, we show that using semiconductor/metal (Schottky) junctions can be used as LAESs and explore their use as sensors for dopamine. This configuration is attractive because it allows for simple preparation of LAESs and enables the direct measurement of freely diffusing redox couples. Although the Au NPs covered only ∼30% of the sensor

https://dx.doi.org/10.1021/acs.analchem.0c02512
Anal. Chem. 2020, 92, 11444−11452

surface, we observed fast HET kinetics for FcMeOH oxidation and long-term stability over 1000 CV cycles. We also challenged the LAES to detect the neurotransmitter dopamine and found that the sensors were quantitative over the range from 0.4 to 598 μM in a buffer with an estimated limit of detection of 0.8 μM, demonstrating that these sensors have potential for quantifying freely diffusing neurotransmitters. Additionally, we used local illumination to generate a virtual array of electrochemical sensors for dopamine. We used the virtual array to eliminate total sensor failure during electrochemically induced biofouling, which is a common issue with electrochemical sensing of biologically relevant compounds. The encouraging results presented here establish that Schottky junctions are effective tools for LAESs and should be useful for a number of interesting future applications in chemical and biological sensing.

■ ASSOCIATED CONTENT

Supporting Information

The Supporting Information is available free of charge at https://pubs.acs.org/doi/10.1021/acs.analchem.0c02512.

Additional text and figures describing EDX analysis of n-Si/AuNP samples; Mott−Schottky analysis of n-Si/AuNP samples; comparison of n-Si/AuNP samples with different electrodeposition times; additional electrochemical characterization of n-Si/AuNP samples and control measurements using freshly etched n-Si; analysis of cyclic voltammetry stability experiments in 1 mM FcMeOH; additional dopamine fouling experiments; image and description of local illumination setup; Figures S1−S13 (PDF)

■ AUTHOR INFORMATION

Corresponding Author

Glen D. O'Neil − *Department of Chemistry and Biochemistry, Montclair State University, Montclair, New Jersey 07043, United States;* orcid.org/0000-0002-2252-779X; Email: oneilg@montclair.edu

Authors

Irina M. Terrero Rodríguez − *Department of Chemistry and Biochemistry, Montclair State University, Montclair, New Jersey 07043, United States*

Alexandra J. Borrill − *Department of Chemistry and the Centre for Doctoral Training in Diamond Science and Technology, University of Warwick, Coventry CV4 7AL, United Kingdom*

Katherine J. Schaffer − *Department of Chemistry and Biochemistry, Montclair State University, Montclair, New Jersey 07043, United States*

Jocelyn B. Hernandez − *Department of Chemistry and Biochemistry, Montclair State University, Montclair, New Jersey 07043, United States*

Complete contact information is available at: https://pubs.acs.org/10.1021/acs.analchem.0c02512

Notes

The authors declare no competing financial interest.

■ ACKNOWLEDGMENTS

We acknowledge support from Montclair State University, the National Science Foundation (NSF CBET-1944432), and the Research Corporation for Science Advancement (Cottrell Scholar). Any opinions, findings, and conclusions or recommendations expressed in this material are those of the author(s) and do not necessarily reflect the views of the National Science Foundation. ITR acknowledges support from Montclair State University and Dominican Republic's Ministry of Higher Education, Science and Technology (MESCyT).

■ REFERENCES

(1) Licht, S.; Myung, N.; Sun, Y. *Anal. Chem.* **1996**, *68* (6), 954−959.
(2) Vogel, Y. B.; Gooding, J. J.; Ciampi, S. *Chem. Soc. Rev.* **2019**, *48*, 3723−3739.
(3) Walter, M. G.; Warren, E. L.; McKone, J. R.; Boettcher, S. W.; Mi, Q.; Santori, E. A.; Lewis, N. S. *Chem. Rev.* **2010**, *110*, 6446−6473.
(4) Lewis, N. S. *Inorg. Chem.* **2005**, *44* (20), 6900−6911.
(5) Lewis, N. S. *Acc. Chem. Res.* **1990**, *23* (1), 176−183.
(6) Santangelo, P. G.; Miskelly, G. M.; Lewis, N. S. *J. Phys. Chem.* **1988**, *92* (22), 6359−6367.
(7) Santangelo, P. G.; Miskelly, G. M.; Lewis, N. S. *J. Phys. Chem.* **1989**, *93*, 6128−6136.
(8) Santangelo, P. G.; Lieberman, M.; Lewis, N. S. *J. Phys. Chem. B* **1998**, *102*, 4731−4738.
(9) Bard, A. J.; Faulkner, L. R. *Electrochemical Methods: Fundamentals and Applications*, Second Edi.; John Wiley & Sons, Inc.: New York, 2001.
(10) Choudhury, M. H.; Ciampi, S.; Yang, Y.; Tavallaie, R.; Zhu, Y.; Zarei, L.; Goncales, V. R.; Gooding, J. J. *Chem. Sci.* **2015**, *6* (12), 6769−6776.
(11) Yang, Y.; Cuartero, M.; Goncales, V. R.; Gooding, J. J.; Bakker, E. *Angew. Chem., Int. Ed.* **2018**, *57*, 16801−16805.
(12) Lian, J.; Yang, Y.; Wang, W.; Parker, S. G.; Goncales, V. R.; Tilley, R. D.; Gooding, J. J. *Chem. Commun.* **2019**, *55*, 123−126.
(13) Wu, F.; Zhou, B.; Wang, J.; Zhong, M.; Das, A.; Watkinson, M.; Hing, K.; Zhang, D.-W.; Krause, S. *Anal. Chem.* **2019**, *91*, 5896−5903.
(14) Chung, T. D.; Lim, S. Y.; Kim, Y.-R.; Ha, K.; Lee, J.-K.; Lee, J. G.; Jang, W.; Lee, J.-Y.; Bae, J. H. *Energy Environ. Sci.* **2015**, *8*, 3654−3662.
(15) Lim, S. Y.; Han, D.; Kim, Y.; Chung, T. D. *ACS Appl. Mater. Interfaces* **2017**, *9*, 23698−23706.
(16) Vogel, Y. B.; Zhang, L.; Darwish, N.; Goncales, V. R.; Le Brun, A.; Gooding, J. J.; Molina, A.; Wallace, G. G.; Coote, M. L.; Gonzalez, J.; Ciampi, S. *Nat. Commun.* **2017**, *8*, 2066.
(17) Goncales, V. R.; Lian, J.; Gautam, S.; Tilley, R. D.; Gooding, J. J. *Annu. Rev. Anal. Chem.* **2020**, *13*, 135.
(18) Lancaster, M.; Alqurashi, A.; Selvakumar, C. R.; Maldonado, S. *J. Phys. Chem. C* **2020**, *124*, 5021−5035.
(19) Yang, Y.; Ciampi, S.; Choudhury, M. H.; Gooding, J. J. *J. Phys. Chem. C* **2016**, *120*, 2874.
(20) Ahmad, S.; Ciampi, S.; Parker, S.; Goncales, V. R.; Gooding, J. J. *ChemElectroChem* **2019**, *6*, 211.
(21) Choudhury, M. H.; Ciampi, S.; Lu, X.; Kashi, M. B.; Zhao, C.; Gooding, J. J. *Electrochim. Acta* **2017**, *242*, 240−246.
(22) Yang, Y.; Ciampi, S.; Gooding, J. J. *Langmuir* **2017**, *33*, 2497−2503.
(23) Parker, S. G.; Yang, Y.; Ciampi, S.; Gupta, B.; Kimpton, K.; Mansfeld, F.; Kavallaris, M.; Gaus, K.; Gooding, J. J. *Nat. Commun.* **2018**, *9*, 2288.
(24) Kashi, M. B.; Wu, Y.; Goncales, V. R.; Choudhury, M. H.; Ciampi, S.; Gooding, J. J. *Electrochem. Commun.* **2016**, *70*, 28−32.
(25) Kashi, M. B.; Silva, S. M.; Yang, Y.; Goncales, V. R.; Parker, S. G.; Barfidokht, A.; Ciampi, S.; Gooding, J. J. *Electrochim. Acta* **2017**, *251*, 250−255.
(26) Seo, D.; Lim, S. Y.; Lee, J.; Yun, J.; Chung, T. D. *ACS Appl. Mater. Interfaces* **2018**, *10*, 33662−33668.
(27) Saada, H.; Abdallah, R.; Bergamini, J.-F.; Fryars, S.; Dorcet, V.; Joanny, L.; Gouttefangeas, F.; Ollivier, S.; Loget, G. *ChemElectroChem* **2020**, *7* (5), 1155−1159.

(28) Zhao, S.; Völkner, J.; Riedel, M.; Witte, G.; Yue, Z.; Lisdat, F.; Parak, W. J. *ACS Appl. Mater. Interfaces* **2019**, *11*, 21830−21839.
(29) Yue, Z.; Lisdat, F.; Parak, W. J.; Hickey, S. G.; Tu, L.; Sabir, N.; Dorfs, D.; Bigall, N. C. *ACS Appl. Mater. Interfaces* **2013**, *5*, 2800−2814.
(30) Esposito, D. V.; Levin, I.; Moffat, T. P.; Talin, A. A. *Nat. Mater.* **2013**, *12* (6), 562−568.
(31) Scheuermann, A. G.; Lawrence, J. P.; Kemp, K. W.; Ito, T.; Walsh, A.; Chidsey, C. E. D.; Hurley, P. K.; McIntyre, P. C. *Nat. Mater.* **2016**, *15*, 99−105.
(32) Tung, R. T. *Phys. Rev. B: Condens. Matter Mater. Phys.* **1992**, *45* (23), 13509−13523.
(33) Lubin, A. A.; Plaxco, K. W. *Acc. Chem. Res.* **2010**, *43* (4), 496−505.
(34) Simcox, L. J.; Pereira, R. P. A.; Wellington, E. M. H.; Macpherson, J. V. *ACS Appl. Mater. Interfaces* **2019**, *11*, 25024−25033.
(35) Barfidokht, A.; Gooding, J. J. *Electroanalysis* **2014**, *26*, 1182−1196.
(36) Patel, A. N.; Tan, S.-Y.; Miller, T. S.; Macpherson, J. V.; Unwin, P. R. *Anal. Chem.* **2013**, *85*, 11755−11764.
(37) Peltola, E.; Sainio, S.; Holt, K. B.; Palomaki, T.; Koskinen, J.; Laurila, T. *Anal. Chem.* **2018**, *90*, 1408−1416.
(38) Hanssen, B. L.; Siraj, S.; Wong, D. K. Y. *Rev. Anal. Chem.* **2016**, *35* (1), 1−28.
(39) Prod'Homme, P.; Maroun, F.; Cortès, R.; Allongue, P. *Appl. Phys. Lett.* **2008**, *93* (17), 171901.
(40) Chen, Q.; Switzer, J. A. *ACS Appl. Mater. Interfaces* **2018**, *10* (25), 21365−21371.
(41) Gelderman, K.; Lee, L.; Donne, S. W. *J. Chem. Educ.* **2007**, *84* (4), 685.
(42) Acharya, S.; Lancaster, M.; Maldonado, S. *Anal. Chem.* **2018**, *90*, 12261−12269.
(43) McCreery, R. L. *Chem. Rev.* **2008**, *108* (7), 2646−2687.
(44) Ammann, D.; Pretsch, E.; Simon, W.; Lindner, E.; Bezegh, A.; Pungor, E. *Anal. Chim. Acta* **1985**, *171*, 119−129.
(45) Park, J. H.; Thorgaard, S. N.; Zhang, B.; Bard, A. J. *J. Am. Chem. Soc.* **2013**, *135*, 5258−5261.
(46) Vogel, Y. B.; Molina, A.; Gonzalez, J.; Ciampi, S. Quantitative Analysis of Cyclic Voltammetry of Redox Monolayers Adsorbed on Semiconductors: Isolating Electrode Kinetics, Lateral Interactions, and Diode Currents. *Anal. Chem.* **2019**.*915929*
(47) Nicholson, R. S. *Anal. Chem.* **1965**, *37*, 1351−1355.
(48) Velicky, M.; Bradley, D. F.; Cooper, A. J.; Hill, E. W.; Kinloch, I. A.; Mishchenko, A.; Novoselov, K. S.; Patten, H. V.; Toth, P. S.; Valota, A. T.; Worrall, S. D.; Dryfe, R. A. W. *ACS Nano* **2014**, *8*, 10089−10100.
(49) Lavagnini, I.; Antiochia, R.; Magno, F. *Electroanalysis* **2004**, *16* (6), 505−506.
(50) Pourbaix, M. *Atlas of Electrochemical Equilibria in Aqueous Solutions*, First.; Pergamon Press: New York, 1966.
(51) Hill, C. M.; Kim, J.; Bard, A. J. *J. Am. Chem. Soc.* **2015**, *137*, 11321−11326.
(52) Scheuermann, A. G.; McIntyre, P. C. Atomic Layer Deposited Corrosion Protection: A Path to Stable and Efficient Photoelectrochemical Cells. *J. Phys. Chem. Lett.* **2016**, acs.jpclett.6b00631.72867
(53) Oh, K.; Meriadec, C.; Lassalle-Kaiser, B.; Dorcet, V.; Fabre, B.; Ababou-Girard, S.; Joanny, L.; Gouttefangeas, F.; Loget, G. *Energy Environ. Sci.* **2018**, *11*, 2590−2599.
(54) Digdaya, I. A.; Trzesniewski, B. J.; Adhyaksa, G. W. P.; Garnett, E. C.; Smith, W. A. *J. Phys. Chem. C* **2018**, *122* (10), 5462−5471.
(55) Robinson, D. L.; Hermans, A.; Seipel, A. T.; Wightman, R. M. *Chem. Rev.* **2008**, *108* (7), 2554−2584.
(56) Armbruster, D. A.; Pry, T. *Clin. Biochem. Rev.* **2008**, *29* (Suppl), S49−S52.
(57) Mocak, J.; Bond, A. M.; Mitchell, S.; Scollary, G. *Pure Appl. Chem.* **1997**, *69* (2), 297−328.
(58) Kalinke, C.; Neumsteir, N. V.; Aparecido, G. de O.; Ferraz, T. V. de B.; dos Santos, P. L.; Janegitz, B. C.; Bonacin, J. A. *Analyst* **2020**, *145*, 1207−1218.
(59) Bucher, E. S.; Wightman, R. M. *Annu. Rev. Anal. Chem.* **2015**, *8* (1), 239−261.
(60) Venton, B. J.; Cao, Q. *Analyst* **2020**, *145* (4), 1158−1168.
(61) Zachek, M. K.; Hermans, A.; Wightman, R. M.; Mccarty, G. S. *J. Electroanal. Chem.* **2008**, *614*, 113−120.
(62) Vogel, Y. B.; Goncales, V. R.; Gooding, J. J.; Ciampi, S. *J. Electrochem. Soc.* **2018**, *165*, H3085−H3092.
(63) Goncales, V. R.; Lian, J.; Gautam, S.; Hagness, D.; Yang, Y.; Tilley, R. D.; Ciampi, S.; Gooding, J. J. *J. Phys. Chem. C* **2020**, *124*, 836.

https://dx.doi.org/10.1021/acs.analchem.0c02512
Anal. Chem. 2020, 92, 11444−11452